Macromolecules

Article

pubs.acs.org/Macromolecules

Kinetic Process of Shish Formation: From Stretched Network to Stabilized Nuclei

Kunpeng Cui,[†] Zhe Ma,[‡] Zhen Wang,[†] Youxin Ji,[†] Dong Liu,[†] Ningdong Huang,[†] Liang Chen,[†] Wenhua Zhang,*[,†] and Liangbin Li*[,†]

[†]National Synchrotron Radiation Lab and College of Nuclear Science and Technology, CAS Key Laboratory of Soft Matter Chemistry, University of Science and Technology of China, Hefei, China

[‡]School of Material Science and Engineering, Tianjin University, Tianjin 300072, China

Supporting Information

ABSTRACT: On the basis of the duality of the shish-kebab superstructure, coil−stretch transition (CST) is well recognized as the molecular mechanism for shish-kebab formation in polymer melts, which, however, is challenged by recent results in flow-induced crystallization (FIC). In this work, we perform a real time investigation on FIC of polyethylene bimodal blends by combing a unique homemade extensional rheometer and synchrotron radiation small-angle X-ray scattering. The results show that the critical strain for shish formation decreases with increasing long chain concentration, which contradicts the role of CST but agrees well with stretched network model (SNM). Quantitative analyses indicate that the formation of shish is determined by the degree of network deformation rather than solely by strain or long chain concentration at a specific temperature. In addition, three types of shish with different stability are observed sequentially by increasing strain. On the basis of our results, strong support is given to the idea that shish formation is a kinetic process. When stretched to a critical deformation degree, the aligned segments couple with each other to form fibrillar-like type I shish, which further transform into type II shish embedded with sporadic lamellae and type III shish embedded with well-defined periodic lamellae sequentially by increasing flow intensity. Our results and the resulting conceptual model not only demonstrates that shish formation is derived from SNM but unveils its kinetic process from initial chain configuration to final stable nuclei.

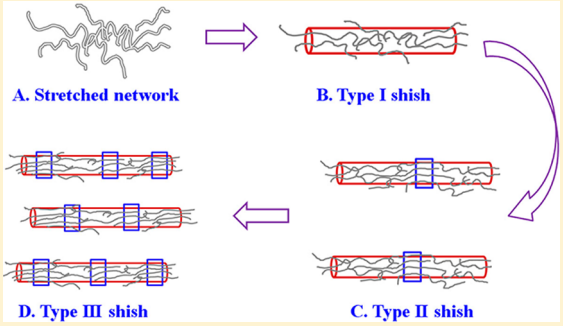

INTRODUCTION

The subject of flow-induced crystallization (FIC) in polymer melts is of vital importance not only in scientific research but also in industrial application. In most common scenarios flow is inevitably involved during polymer processing, which dictates subsequent morphologies and thus end-use properties of materials.[1,2] The most dramatic change in morphology associated with flow is the transition from isotropic spherulite to highly orientated shish-kebab structure with notably increased stiffness and strength.[3−7] Shish-kebab comprises of central threadlike core, namely, shish which is encircled by disk-like crystals, namely kebabs. Although has been observed for several decades, the exact molecular mechanism for shish-kebab formation still remains unclear and under open debates.

Two molecular mechanisms, the coil−stretch transition (CST)[8] and stretched network model (SNM)[9] are well recognized for shish-kebab formation. The CST was first proposed by de Gennes in investigating chain dynamic of polymer solution under flow.[10] Keller provided birefringent evidence for the existence of CST and attributed it to the subsequent shish-kebab formation in polymer solution.[11] Then the CST was further extended to polymer melt as the shish-kebab morphology formed in melt is analogous to that in solution.[8,12] According to CST, the longest chains can be stretched to transform into shish and the rest shorter ones stay as coil state to crystallize as kebab. Soon afterward, bimodal blends comprised of small amounts of long chains in short-chain matrix were widely used to verify the mechanism of shish-kebab formation.[13−21] However, it should be aware that the CST derived from solution lacks the strict physical basis in melts as the essential ingredient hydrodynamic effect in solution does not exist in melt. In addition, report on shish consisting of both short and long chains in melts by Kornfield et al. also contradicts the validly of CST in shish formation.[4] Long chains with concentration equal or above overlap concentration (c^*) is a precondition for shish formation in bimodal blends, implying that long chains should be stretched as an entangled network rather than single-chains behavior under flow.[15,17,22] Here the network represents the transient network constructed with entangled chains which is similar to network material containing cross-links. Furthermore, both in situ rheo-SAXS and optical results seemed coincident with the

Received: April 19, 2015
Revised: July 24, 2015
Published: July 31, 2015

DOI: 10.1021/acs.macromol.5b00819
Macromolecules 2015, 48, 5276−5285

view of stretched network recently.[23−25] Nevertheless, due to experimental difficulty, direct evidence to demonstrate that the stretched network is responsible for shish formation in polymer melts is still absent.

No matter in CST or SNM, only correspondence between initial chain conformations and final crystal morphologies is proposed. Nevertheless, less attention has been paid to the process how stretched chains or network transform into shish. This process is challenging to study because of fast dynamic. While the temperature or flow intensity dependent evolution of flow-induced structures such as shish or precursors may partially reflect the essential features of this process. Memory experiments revealed that the structures induced by flow have a lifetime of several hours in superheated melts and follow an Arrhenius-type relaxation model with temperature.[26,27] Time-resolved X-ray scattering results suggested the existence of precursor, which may dissolve into melts or transform into stable shish depending on its size.[5] The appearance of precursor for shish formation was further supported by recent ultrafast X-ray and polarized optical microscope studies.[28−31] Although more and more experimental results imply the indirect transformation from chain conformations to shish nuclei, however, the lack of effective and systemic evidence leave this process still obscure. Ingenious experiments and sophisticated instruments are needed to illuminate this long-standing problem of molecular mechanism for shish-kebab formation, or specifically to two essential questions, (i) Is CST or SNM responsible for shish formation in polymer melts? (ii) How shish forms from the initial coiled chain conformation to final stabilized nuclei?

In this work, bimodal blends consisting of two linear polyethylene (PE) samples with low molecular weight (LMW) and ultrahigh molecular weight (UHMW) are prepared with only UHMW component is expected to meet the requirement of chain stretch as a precondition for shish formation. The scaling law between entanglement molecular weight and concentration of UHMW component is utilized with tact to test the mechanism of shish formation. In case SNM holds true, the strain to stretch the segments between adjacent entanglements should follow the same scaling law. Thus, the validity of CST or SNM can be judged from the critical strain for shish formation whose dependence on UHMW component concentration is different. The critical strain for shish formation can be obtained by combing a homemade extensional rheometer and synchrotron radiation small-angle X-ray scattering (SAXS). A relative high extension temperature is selected to highlight nucleation under flow at which growth rate of crystal is negligible. With delicately designed thermal history, the formation process of shish can be deduced by monitoring the structure evolution at different strains, i.e., different stage of shish formation. Our results show that the critical strain for shish formation decrease with increasing UHMW component concentration, which is fitted with the stretched network model well. In addition, three types of shish can be identified by increasing strain, exhibiting as different stages in the formation of stabilized shish nuclei.

EXPERIMENTAL SECTION

Materials and Sample Preparation. LMW PE with weight and number-average molecular weight (M_w and M_n) of about 823 and 42 kg/mol respectively (Figure S1, Supporting Information), and UHMW PE with M_w of about 6000 kg/mol are used in this study. A relative wide molecular weight distribution of LMW PE is chosen because of the requirement of melt strength for extensional experiment, but it does not affect our analysis as demonstrated in the Discussion. Bimodal blends with different UHMW PE concentrations are prepared by solution blending to ensure the intimate mixing at molecular level. The blending procedure is listed as following. Mixture of LMW and UHMW PEs is first dissolved in xylene to form a homogeneous solution and then held at 130 °C with continuous stirring for 1.5 h under a nitrogen atmosphere. Precipitate of polymer blends is obtained by pouring the solution into cold methanol with continuous stirring. Then the blend slurry is filtered and dried in a vacuum at 80 °C for 3 days to remove residual solvent. Control sample of pure LMW PE is also prepared as reference material using the same aforementioned procedure.

All concentrations of UHMW PE in the blends (1, 2, 5, and 10 wt %) designed are larger than the c^*, aiming to construct UHMW PE entangled network in LMW PE matrix. For PE with M_w of 480 kg/mol, c^* is estimated as 0.028 wt %.[23] The precipitates are molded to films of 1 mm thickness by a vacuum press at 180 °C and cut into rectangular shape with dimensions of 30 × 18 × 1 mm^3 for extension experiments. B0, B1, B2, B5, and B10 are used to represent samples with UHMW PE concentration of 0, 1, 2, 5, and 10 wt %, respectively. The nominal melting temperatures for quiescently crystallized B0 and B10 samples are almost same (about 133 °C) from Differential scanning calorimetry (DSC) measurements, indicating the addition of UHMW component has negligible influence on the melting point (Figure S2, Supporting Information).

Instrumentation. A homemade extensional rheometer is used to provide well-defined thermal history and extensional flow field (Figure 1a). The detailed description of this device has been reported

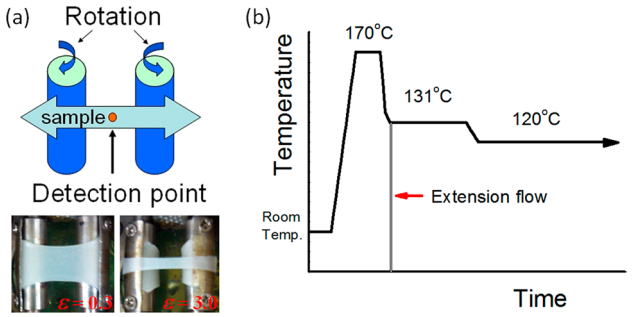

Figure 1. (a) Schematic drawing of the extensional rheometer and photographs of PE samples after subjected to strain of 0.3 and 3.0, respectively. (b) Procedure of the applied thermo-mechanical history.

elsewhere.[32] The design of this device is similar to the commercial Sentmanat extensional rheometer, which allows us to obtain Hencky strain. The ends of sample are mechanically fixed to two drums, which can rotate reversely with same velocity by gear drive. The two drums have a diameter of 10 mm and axis-to-axis distance of 20 mm. During test, the length of the sample for extension keeps constant and equals to the axis-to-axis distance. Thus, with a constant velocity of the drum surface, the strain rate is constant. Combing this device with X-ray scattering, not only strain rate and strain can be controlled independently, but also direct rheological and structural data can be obtained. While those functions cannot be reached at the same time by existing extensional flow technique such as opposed jet device[8] or four-roll mill flow chamber.[33] Time-resolved SAXS measurements are performed at the BL16B beamline of the Shanghai Synchrotron Radiation Facility (SSRF). The wavelength of X-ray and the distance of sample to detector are 0.124 nm and 5400 mm, respectively. Two dimensional (2D) scattering images are collected with a Mar165 CCD detector (2048 × 2048 pixels with pixel size of 80 μm) and analyzed with Fit2D software from European Synchrotron Radiation Facility.[34] The data acquisition time and the storage time are 10 and 5 s respectively for each SAXS pattern.

Experimental Procedures. Each sample is initially heated to 170 °C for 10 min to erase thermal history. Afterward, samples are applied

DOI: 10.1021/acs.macromol.5b00819
Macromolecules 2015, 48, 5276−5285

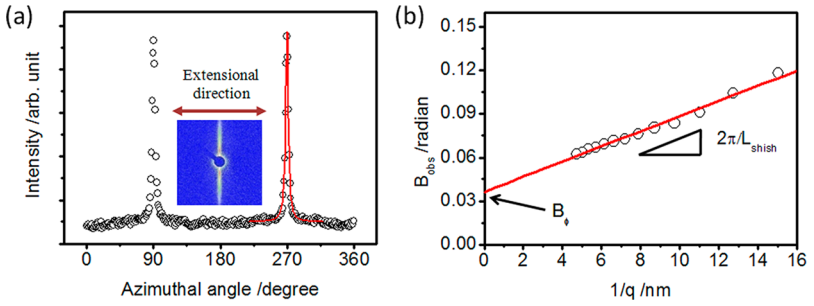

Figure 2. (a) Example of the Lorentzian fitting to the azimuthal scan of SAXS pattern. The extensional direction is meridianal. (b) Plots of azimuthal width (B_{obs}) as a function of $1/q$, which is used to determine average length of shish L_{shish} and the orientation parameter (B_ϕ).

to the thermo-mechanical history schematized in Figure 1b. This procedure can be divided into three steps. The relaxed polymer melt is first cooled to 131 °C with cooling rate about 5 °C/min for extension. The temperature chosen herein is just slightly lower than the melting point, which aims to study the effect of flow on nucleation because crystal growth rate is undetectably slow at this temperature. After reaching 131 °C, a designed strain and strain rate are imposed on the sample. For each UHMW component concentration, the strain rate remains at 3.14 s^{-1} while the strain varies from 0 to 3.5. Then the sample is held at 131 °C for 1800 s to observe the evolution of structure. After 1800 s is elapsed, the sample is finally cooled to 120 °C for isothermal crystallization. Temperature stability is maintained within ±0.5 °C and a nitrogen gas flow is used to homogenize temperature and prevent sample from degradation. In this work, we only discuss the flow-induced nucleation and subsequent isothermal processes at 131 °C. The results of final isothermal crystallization at 120 °C will be delivered in follow-up work.

Data Analysis. All SAXS data are first corrected for background scattering, synchrotron radiation X-ray beam fluctuation and detector spatial distortion. Then 2D SAXS patterns are sector integrated to obtain the scattered intensity $I(q)$ as a function of $q = 4\pi \sin\theta/\lambda$ (Figure 6a), where q is the module of scattering vector, 2θ the scattering angle and λ the wavelength of X-ray. The integrated intensity I_{int} is obtained by summing up the $I(q)$ in the whole accessible q range in the detector $I_{int} = \int I(q)\,dq$. The relative content of shish after extension (t = 10 s) is defined as $\phi_{shish} = (I_{int}^{eq}(0) - I_{int}^{bg})/I_{int}^{bg}$, where $I_{int}^{eq}(0)$ is the equatorial section integrated intensity after cessation of extension and I_{int}^{bg} the background integrated intensity. The relative change of equatorial or meridional section integrated intensity is defined as $\Delta I = (I_{int}(t) - I_{int}(0))/I_{int}(0) - I_{int}^{bg})$, here $I_{int}(t)$ can be equatorial ($I_{int}^{eq}(t)$) or meridional $I_{int}^{me}(t)$ section integrated intensity at time t. Ruland streak method[6,35] is employed to analyze scattering streak in 2D SAXS pattern. The experimentally measured azimuthal breadth of streak (B_{obs}) is a function of the average length L_{shish} and orientation parameter B_ϕ of shish. If Lorentzian profile can be used to describe the orientation distribution, the relation is $B_{obs} = (2\pi/(\langle L_{shish}\rangle q)) + B_\phi$; here, B_{obs} is the integral width from the SAXS streak at q. All results in this study are well fitted with Lorentz functions as demonstrated in Figure 2a. On the basis of above equation, L_{shish} and B_ϕ can be obtained. Figure 2b gives an example of this method to determine those two parameters.

RESULTS

Figure 3 illustrates the rheological data, i.e., engineering stress–Hencky strain plots of various UHMW PE concentrations (B0, B1, B2, B5, and B10) at 131 °C during step extensional flow. For B0, the stress first increases almost linearly with strain and then shows an overshot. After exceeding overshot, the stress shows a decline process followed by a stress-upturn finally. The stress evolutions of other UHMW PE concentrations also show similar behaviors as that of B0. However, both the magnitude of stress and the onset strain for stress-upturn are affected by increasing UHMW PE concentration. As an instance, the

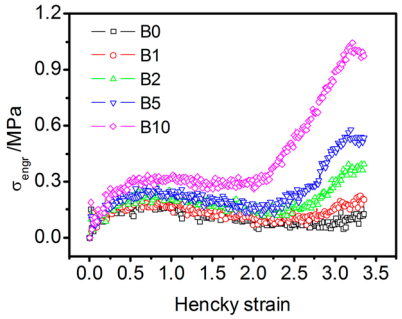

Figure 3. Engineering stress (σ_{engr}) as a function of Hencky strain for bimodal blends with different UHMW PE concentration at 131 °C.

maximum stress and the onset strain for stress-upturn increase from 0.14 MPa and 2.9 for B0 to 1.05 MPa and 2.0 for B10. The occurrence of stress-upturn indicates that viscosity changes during flow, which may be attributed to chain stretch a precondition for shish formation. Meanwhile, the onset strain for stress-upturn decreases with increasing UHMW PE concentration.

The speculation of chain stretch during flow is evidenced by the appearance of shish scattering, which is a straightforward fingerprint to the pre-existing state of chain stretch. The selected 2D SAXS patterns for samples with different strain and UHMW component concentration after cessation of extension (t = 10 s) are presented in Figure 4. Two types of scattering patterns are observed with the boundary marked by a red

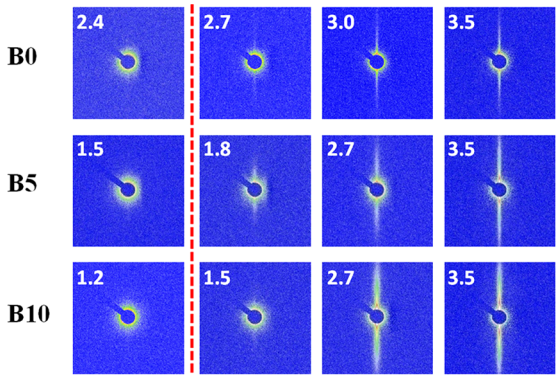

Figure 4. Selected 2D SAXS patterns after cessation of extensional flow (t = 10 s) for samples with various UHMW PE concentration and different strain at 131 °C. The strain rate keeps constant at 3.14 s^{-1}. The number at the left corner of each pattern represents the value of strain, and the red dashed line guides the eye to the appearance of streak scattering.

DOI: 10.1021/acs.macromol.5b00819
Macromolecules 2015, 48, 5276−5285

dashed line. On the right side of the red line, scattering streaks perpendicular to the extension direction appear as a sign of formation of shish structure which has strong electron density contrast to surrounding molten matrix. Shish develops in all blends from B0 to B10, while the onset strain for shish formation and the magnitude of shish scattering depend on UHMW component concentration. For B0, shish scattering arises at a strain of 2.7, which decreases to 1.8 for B5. Though discernible, the streak scattering is very weak for B0 with a strain of 2.7. While for B5, strong streak scattering is exhibited at the same strain. On the left side of the red line only diffused scattering is shown, suggesting the absence of any detectable structure.

The relative content of shish ϕ_{shish} following cessation of step extension (t = 10 s) is extracted from the streak scattering in 2D SAXS patterns with the method described above. The critical strain for shish formation is determined by the plot of ϕ_{shish} vs strain as demonstrated in Figure 5. The critical strain

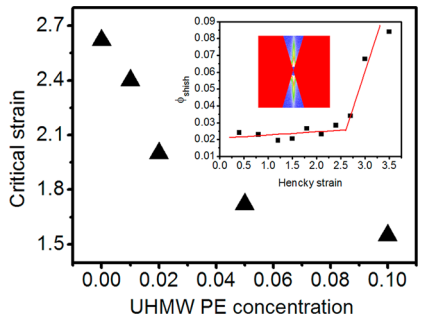

Figure 5. Critical strain for shish formation at different UHMW PE concentration at 131 °C. The inset show an example of the method to determine the critical strain.

for shish formation decreases with the increase of UHMW component concentration, similar to the evolutionary trend of onset strain for stress-upturn but with smaller value. For example, the critical strains for B0 and B10 for shish formation are 2.6 and 1.55, which increase to 2.9 and 2.0 for stress-upturn.

Although shish nuclei can be induced at different strains for a specific UHMW component concentration, the detailed structure of shish in fact varies with strain. Three types of shish can be defined according to the structure evolution data during isothermal process at 131 °C. As the structure evolution at different UHMW component concentrations share similar trends for an assigned type of shish, only the results of B5 are presented for demonstration. SAXS data during isothermal process at 131 °C with a strain of 2.4 for B5 are exhibited in Figure 6 to illustrate the nature of shish named type I. Two selected 2D SAXS patterns at the beginning (10 s) and the end (1800 s) of the isothermal process show no obvious change except for a slight attenuation in the intensity of streak scattering. The relative change of integrated intensities in equatorial and meridional sections (ΔI_{eq} and ΔI_{me}) can be extracted with the aforementioned method based on 2D scattering patterns. Indeed ΔI_{eq} (shish scattering) weakly decays resulting in a total relative decrement of about 2.0%, which is accompanied by shortening in average length of shish from 456 to 365 nm (Figure 6c). No detectable lamellar scattering appears in meridional region in 2D SAXS pattern even at 1800 s (Figure 6a), which is also supported by the absence of scattering maximum in 1D SAXS intensity profiles in Figure 6d (the contribution of amorphous melt scattering is subtracted in Figure 6d to make the scattering signal more obvious if new structure forms). Meanwhile, ΔI_{me} has almost no change during the whole isothermal process even though ΔI_{eq} decreases with time.

An example of B5 sample with a strain of 2.7 is shown in Figure 7 to convey the feature of shish named type II. Different from the type I shish, the streak scattering in 2D SAXS patterns at 1800 s is slightly stronger than that at 10 s as shown in Figure 7a. Further analysis indicates increment of ΔI_{eq} about 4% at the end of isothermal process (Figure 7b). The average length of shish L_{shish} still decreases as demonstrated in Figure 7c. L_{shish} at the beginning and the end of isothermal process are 616 and 426 nm, respectively, larger than those at strain of 2.4. B_{ϕ} decreases gradually with proceeding isothermal time (Figure 7c), suggesting an improvement of the orientation degree of shish. Both the 2D SAXS pattern (Figure 7a) and 1D intensity

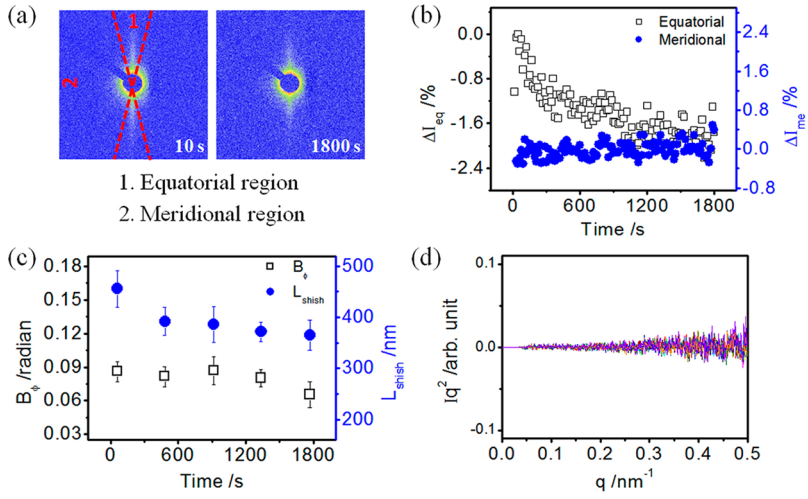

Figure 6. SAXS data during isothermal process at 131 °C for B5 sample with a strain of 2.4. (a) 2D selected SAXS patterns at the beginning and the end of isothermal process. The red dashed lines donate the boundary to define the equatioral and meridional regions. (b) Relative change of equatorial and meridional sections integrated intensities (ΔI_{eq} and ΔI_{me}), (c) average length of shish (L_{shish}) and orientation paramter (B_{ϕ}), and (d) 1D SAXS intensity profiles evolving with time during the isothermal process. In part d, the component of amorphous melt scattering is subtracted.

DOI: 10.1021/acs.macromol.5b00819
Macromolecules 2015, 48, 5276−5285

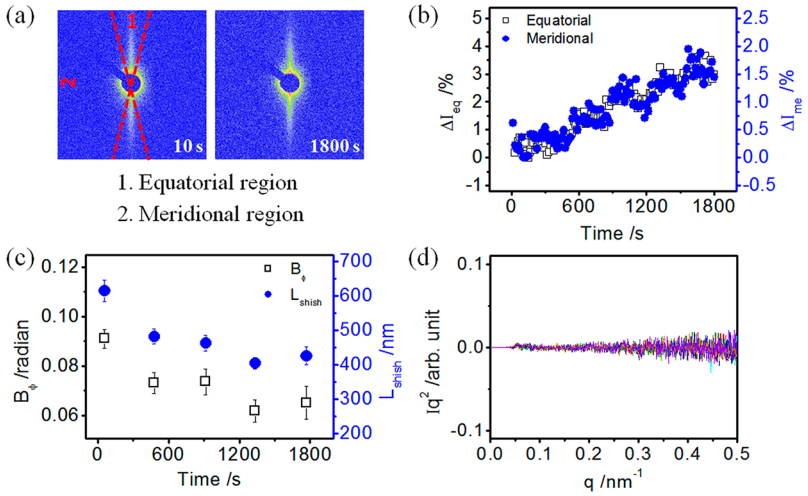

Figure 7. SAXS data during isothermal process at 131 °C for B5 sample with a strain of 2.7. (a) 2D selected SAXS patterns at the beginning and the end of isothermal process. (b) Relative change of equatorial and meridional sections integrated intensities (ΔI_{eq} and ΔI_{me}), (c) average length of shish (L_{shish}) and orientation parameter (B_ϕ), and (d) 1D SAXS intensity profiles evolving with time during the isothermal process. In part d, the component of amorphous melt scattering is subtracted.

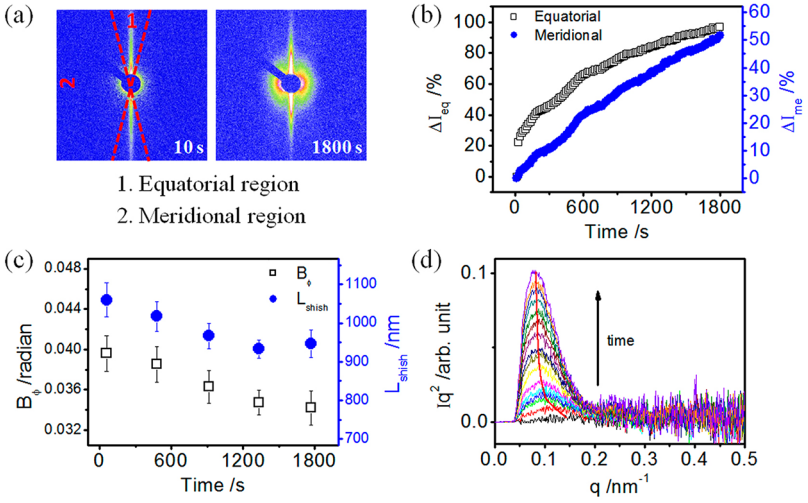

Figure 8. SAXS data during isothermal process at 131 °C for B5 sample with a strain of 3.5. (a) 2D selected SAXS patterns at the beginning and the end of isothermal process. (b) relative change of equatorial and meridional sections integrated intensities (ΔI_{eq} and ΔI_{me}), (c) average length of shish (L_{shish}) and orientation parameter (B_ϕ), and (d) the 1D SAXS intensity profiles evolving with time during the isothermal process. In part d, the component of melt amorphous scattering is subtracted.

profiles (Figure 7d) suggest that no detectable periodic lamellar structure appears, but ΔI_{me} increases by increasing time with a value of about 2% at the end of isothermal process (Figure 7b). Interestingly, an exact positive correlation exists between ΔI_{me} and ΔI_{eq}, indicating that they may be stemmed from same structure.

New characters of type III shish are discovered in B5 sample with a strain of 3.5, which display remarkably stronger streak scattering in 2D SAXS pattern at 1800 s than that at 10 s in Figure 8a. From Figure 8b, a significant increment is observed in ΔI_{eq}, which reaches 97% at the end of isothermal process, much larger than −2.0% for type I shish with strain of 2.4 and 4.0% for type II shish with strain of 2.7. Similar to the two types of shish mentioned above, the average length of the type III shish also decreases with time while accompanied by an increment in orientation degree (Figure 8c). The most noteworthy feature of the type III shish is that scattering maximum appears in extensional direction in 2D SAXS pattern (Figure 8a), suggesting the formation of well-defined lamellar structure with lamellar normal orientated along the flow direction. Simultaneously, a scattering peak presents in the 1D intensity profiles in Figure 8d, which growths with time. In addition, the peak position shifts to the low q side as highlighted by the red curve, indicating elongated average periodicity of lamellar structure with time. The long period extends from about 44 nm after extension to about 76 nm at the end of isothermal process. It should be noted that the lamellar structure appear here is different from the common kebab structure, the former is embed in shish structure while the later is generated from lateral growth of shish as nuclei. The detailed reason will be given in the Discussion.

The formation of different types of shish not only depends on the strain as already shown but also on the UHMW component concentration. As exhibited in Figure 9, the onset strain for appearance of the type II shish reduces from 3.5 for B0 to 3.0 for B1. Similarly, the onset strain for type III shish

DOI: 10.1021/acs.macromol.5b00819
Macromolecules 2015, 48, 5276−5285

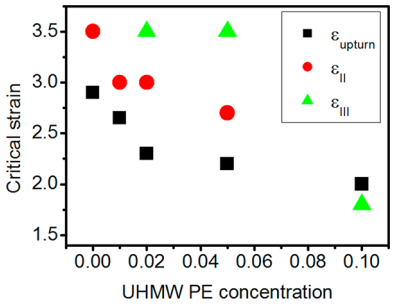

Figure 9. Critical strain for appearance of stress-upturn (ε_{upturn}), type II shish (ε_{II}), and type III shish (ε_{III}) as a function of UHMW PE concentration.

drops from 3.5 for B2 to 1.8 for B10. The type III does not occur in B0 and B1 in the studied strain range. While only type III shish is observed for B10 in the strain range from 1.8 to 3.5. Similar to the onset strain for stress-upturn and critical strain for shish formation, the onset strain for the transition between different types of shish also decreases with UHMW component concentration.

DISCUSSION

Combing the results of extension rheological and time-resolved SAXS measurements of PE bimodal blends, some interesting findings can be extracted. (i) Shish scattering signal appears in all materials studied but the critical strain for observing this characteristic signal decreases with increasing UHMW component concentration. (ii) Three types of shish can be defined according to structure evolution during the subsequent isothermal process at 131 °C. The type I shish is characterized by decreasing shish scattering intensity and no lamellar scattering accompanied by no changes of scattering intensity in equatorial region (lamellar signal region if forms) during isothermal process. The features of type II shish include a small increase of shish scattering, which shows an exact positive correlation with the equatorial region scattering intensity during isothermal process, but no observable lamellar scattering. Lamellar scattering is observed in type III shish accompanied by a dramatic increase in both shish and lamellar scattering intensities. (iii) Stress-upturn appears in rheological data for all materials studied. Similar to the critical strain for shish formation, the onset strain for stress-upturn also decreases with UHMW component concentration. On the basis of those interesting findings, the two key questions related to the formation mechanism of shish aforementioned in the Introduction will be answered.

Shish Formation. The rheological behavior of polymer melts can be characterized by two characteristic time constants, terminal relaxation time τ_d and Rouse relaxation time τ_R. Chain stretch occurs for strain rate $\dot{\varepsilon}$ larger than $1/\tau_R$ and chain orientation occurs for $\dot{\varepsilon}$ in the intermediate region from $1/\tau_d$ to $1/\tau_R$, i.e., $1/\tau_d < \dot{\varepsilon} < 1/\tau_R$.[36,37] Chain stretch is a necessary condition for shish formation and only chains longer than a critical length can be stretched by a given flow field. Shish scattering is observed from B0 to B10, indicating that chain stretch occurs in all blends studied. Thus, it deserves to explain why chain stretch occurs in B0 where no UHMW PE is added. The B0 sample used in this work has a quite broad molecular weight distribution, implying the high molecular weight tail may act as the extra UHMW PE added. Here we make a simple estimation to check whether the UHMW component in B0 can meet the requirement of chain stretch or not. To ensure chain stretch, the $\dot{\varepsilon}$ must be larger than $1/\tau_R$. τ_R can be obtained with the relation of $\tau_R = \tau_e Z^2$, where τ_e is the equilibrium time (7×10^{-9} s at 190 °C) and Z the number of entanglements in chain. For τ_R equals to the reciprocal of $\dot{\varepsilon}$ of 3.14 s^{-1}, the corresponding molecular weight is 4800 kg/mol, which comprise of 4 wt % for the B0 sample (Figure S1, Supporting Information). Thus, the HMW tails in B0 are sufficient to reach the chain-stretch criteria at current flow conditions, as confirmed by the appearances of stress-upturn in rheology as well as shish scattering in X-ray measurements.

After elucidating chain stretch during flow, one can question whether the formation of shish is attributed to the CST or SNM. The possibility of stretched single chains behavior; i.e., CST can be ruled out as follows. Taking the molecular weight of 4800 kg/mol as an example, the extension ratio λ required to stretch the coiled chains into fully extended configuration is about 24, much larger than the maximum value of 14 ($\lambda = \exp(\varepsilon)$) for shish formation in our study (please see the calculation details in the Supporting Information). Therefore, CST may not account for shish formation in PE melts at least with the current model. Instead, the SNM is found to be able to quantitatively interpret our SAXS data.

Under current strain rate, the differences in τ_R bring in different deformation to the LMW and the UHMW components with M_w = 4800 kg/mol as a boundary. So that only orientation occurs in LMW chains but UHMW component is stretched. The concentrations of UHMW component with $M_w \geq 4800$ kg/mol from B0 to B10 are all larger than the overlap concentration c^* of 0.028 wt %. That is to say, besides the LMW component entangled network, the UHMW component forms another entangled network, as commonly recognized in bimodal blends by rheological community.[38,39] Specifically, molecular weight of the entanglement among UHMW component itself can be estimated according to the scaling law:[38,40]

$$M_e(\phi) \approx M_e(1)\phi^{-1.3} \quad (1)$$

where ϕ is concentration of the UHMW component and M_e (1) is entanglement molecular weight in bulk polymer melts. The segments between two adjacent entanglement points undergo nearly affine deformation when dimensionless parameter Weissenberg number $W_i = \dot{\varepsilon}\,\tau_R \geq 1$. In equilibrium Gaussian configuration, the end-to-end distance of this segment is

$$\langle R_G^2 \rangle^{1/2} = \sqrt{N} l \quad (2)$$

where N is the number of Kuhn segments between two adjacent entanglements ($N = M_e/M_{kuhn}$) and l the Kuhn length. With fully extended configuration, the end-to-end distance of this segment is

$$R_{max} = Nl \quad (3)$$

Thus, the extension ratio needed to switch the Gaussian configuration to fully extended configuration is

$$\lambda_{max} = R_{max}/\langle R_G^2 \rangle^{1/2} = \sqrt{N} \quad (4)$$

Considering that entanglement molecular weight in UHMW network is a function of its concentration, the eq 4 can be rewritten as

DOI: 10.1021/acs.macromol.5b00819
Macromolecules 2015, 48, 5276−5285

$$\lambda_{max}(\phi) = \sqrt{N(\phi)} = \sqrt{\frac{M_e(\phi)}{M_{Kuhn}}} = \sqrt{\frac{M_e(1)}{M_{Kuhn}}} \times \phi^{-0.65} \quad (5)$$

To assess the magnitude of segmental stretch required to form shish, $\lambda_{shish}(\phi)$ is defined as the critical elongation for shish formation. The dependence of $\lambda_{shish}(\phi)$ on UHMW PE concentration can be quantified by our results as presented in Figure 10, which can also be fitted with the modified eq 5:

$$\lambda_{shish}(\phi) = \alpha\sqrt{\frac{M_e(1)}{M_{Kuhn}}}(\phi + \phi_0)^{-0.65} \quad (6)$$

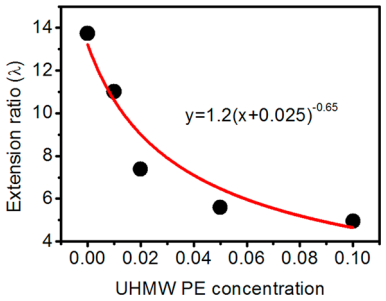

Figure 10. Critical extension ratio for shish formation as a function of UHMW PE concentration at 131 °C. The red line presents the fit with the inserted equation.

where α is a constant describing the relative magnitude of $\lambda_{shish}(\phi)$ to λ_{max}. ϕ_0 is an "effective" concentration of high molecular weight tail that can be stretched at current flow condition in matrix, i.e., the B0 sample. Knowing that $(M_e(1)/M_{Kuhn})$ is 6.9,[41] the two fitting parameters α and ϕ_0 obtained are 0.46 and 0.025, respectively. It is interesting to observe the critical stretch extent of only about 0.46 of the maximum segmental stretch for shish formation, suggesting that the segments between entanglements in UHMW network do not need to be fully extended for shish formation. Instead our discovery indicates that the formation of shish is essentially determined by the degree of network deformation rather than by either strain or UHMW component concentration alone at a specific temperature. In addition, the fitted ϕ_0 = 2.5 wt % coincides with the intrinsic concentration of 4 wt % from GPC data for B0, which further support that the formation of shish is stemmed from stretched network in PE melts.

Determinant for Shish Formation. Factors determine the types of shish in formation process of stabilized shish nuclei will be discussed here. As mentioned above a constant stretch extent of 0.46 for UHMW component network is needed for appearance of shish, which can be explained by the isotropic–nematic transition. That is to say, flow may induce isotropic–nematic transition to form shish (please see the details in Supporting Information). The critical stretch content for appearance of stress-upturn and type II shish are calculated from Figure 9 and presented in Figure 11. Interestingly, both of them keep almost constant within the studied UHMW PE concentration. The critical stretch content of 1 indicates that to form type II shish the segment between adjacent entanglements needs to be fully extended. Note here the deformed unit is Kuhn length in our analysis. The stress-upturn may stem from the formation of shish or intrinsic network effects. For formation of type III shish, the Kuhn segments start to be

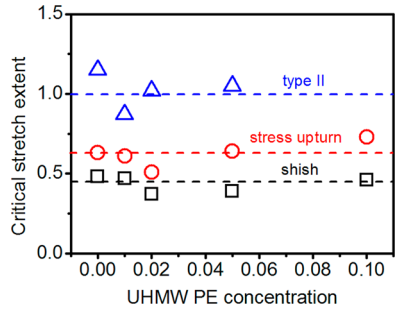

Figure 11. Critical stretch extent for occurrence of different structural signal as a function of UHMW PE concentration. The dashed lines indicate average critical stretch extent measured for specified structural signal.

deformed and it is inappropriate to calculate stretch extent with current definition. The critical stretch content of type III shish is changed with UHMW PE concentration, probably due to structural flow (formation of unstable shish during flow) rather than pure chain deformation.

The shish length generated after cessation of various strains (t = 10 s) are plotted in Figure 12 to understand how shish

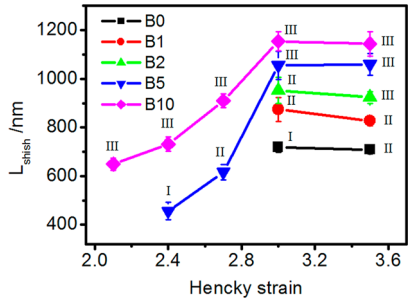

Figure 12. Length of shish at different strain and UHMW PE concentration after cessation of extension (t = 10 s). The I, II and III represent type I, type II, and type III shish, respectively.

develop during flow. It should be mentioned that only shish with good signal/noise ratio can provide values with sufficient accuracy and the shish length is obtained after cessation of extension (t = 10 s). Thus, this calculation just reflects the shish longitudinal growth qualitatively. The complete evolution is obtained for three stages in B5 and subsequent growth for type III in B10. First, it is interesting to find that shish under deformation can grow along the longitudinal direction. Being extended at 3.14 s^{-1}, the longitudinal growth rates before strain of 3.0 are 3.2 and 1.8 μm/s for B5 and B10, respectively, in line with the previous studies of Kornfield et al. in isotactic polypropylene.[14,22] Second, the ultimate shish length increases with increasing UHMPE concentration, consisting with our previous analysis that sample with high UHMW concentration has larger extension degree at the same strain.

Shish Development. Our study also helps to elucidate whether and how the shish evolve further after formation from the initial random coil conformations. Three types of shish are identified with increasing strain, which actually corresponds to the three stages in formation of stabilized shish nuclei. The first stage is type I shish with a decrement of scattering intensity during isothermal process. In general, the decrement of scattering intensity can be caused by the decrease of the volume fraction of the shish or/and the density contrast

DOI: 10.1021/acs.macromol.5b00819
Macromolecules 2015, 48, 5276–5285

between the shish and the surrounding matrix. While it is improbable for the later to happen,[42] the decrement of scattering intensity should be attributed to the decrease in volume fraction of the shish. Indeed the average length of shish decrease with increasing the isothermal time (Figure 6c). This situation can be explained as that some unstable and defective sections of shish relax back to melts due to the internal stress or/and thermal fluctuation, leading to the decrease of average shish length and thus streak scattering intensity. Balzano et al. have already shown that the unstable shish below the critical sizes can relax back to melt during the isothermal process.[5] In the present study, if only very short unstable shish relax, the average shish length should increase. The substantial decrease of average shish length shown here suggests one more relaxation mechanism that defective sections within the long shish, relax and consequently the long shish break into relatively short ones. Interestingly, the equatorial section integrated intensity keeps almost constant during isothermal process, indicating no lamellar structure exists in the shish entity. From the above information a simple scenario one can conclude is that the type I shish is only a fibrillar entity with density larger than the surrounding matrix but without lamellar structure embedded in it (Figure 13B).

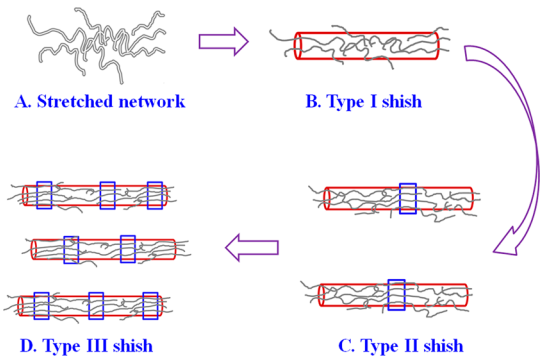

Figure 13. Schematic of kinetic process for shish formation from initial chain conformation to final stable nuclei. (A) Stretched network, (B) type I shish without lamellae, (C) type II shish with sporadic lamellae, and (D) type III shish with periodic lamellae. The flow direction is horizontal.

The distinction of type II shish lies in the formation of lamellar structures inside the shish entity, accounting for the correlation between equatorial section scattering and the shish scattering. But those lamellae structure show no or undetectable periodicity, as evidenced by the absence of scattering maximum in Figure 7d. Similar to type I shish, relaxation of partial defective and less orientated shish leads to the decrease in average shish length and the increase in shish orientation. The increment in scattering intensity for both shish and equatorial section may result from the solidification in some sections of shish to form lamellar structure or the formation of new shish from deformed melts. Even though several possibilities exist, the safe conclusion can be drawn is that the type II shish embraces lamellar structure inside but with no or undetectable periodicity (Figure 13C).

Lamellar structure with well-defined periodicity is observed in the type III shish. One may argue that the periodicity may come from lateral growth of lamellae on shish nuclei. The isothermal temperature chosen here is just slightly lower than the melting point which allows the formation of shish but negligible lateral growth of crystal, as demonstrated by the absence of lamellar or kebab structure during the whole isothermal process for type I shish. Meanwhile, if the periodicity comes from the lateral growth of larger amount of lamella, the scattering intensity of shish should drop due to the decrease in density contrast between shish and surroundings rather than dramatically increase as observed here. Thus, those well-defined lamellar periodicities are mainly from stacks along shish as demonstrated in Figure 13D. The dramatic increment in equatorial scattering intensity (ΔI_{eq} = 97% at 1800 s) during isothermal process may attribute to two reasons. First the perfection of shish contributes to this dramatic increment. Second we deduce that new shish forms during isothermal process. This deduction is further supported by evolution of the 1D intensity profiles in Figure 8d, where the long period of lamellar stacks varies from 44 to 76 nm. The antecedent shish comprises high density of lamellar structures and thus small long period due to the high extension degree of melts. While the later formed shish comprise more dispersed lamellar structures and thus large long period due to the relaxation of the deformed melts. Thereby, the average long period increases with increasing isothermal time. Similar phenomena have been observed and explained in detail in our previous study of poly(ethylene oxide) melts.[43] Meanwhile, the small length of those newly formed shish also leads to a decrease in average length of shish.

As those three types of shish appear sequentially by increasing strain, the type I and II shish can be considered as the intermediate process for formation of type III shish. Combining above discussion on the stretch of UHMW network and different types of shish, a kinetic process for shish formation from initial chain conformation to final stable nuclei is presented in Figure 13. Under external flow, the UHMW component in blends is stretched and deformed as a network (Figure 13A). Once the alignment of segments approaches a critical degree, they will couple to each other and pack into shish bundles. This is why the critical strain for shish formation differs at different UHMW component concentration, because the critical strain to reach the same alignment level (0.46) depends on UHMW component concentration. The shish formed at first stage (type I, Figure 13B) with density contrast to matrix but no embedded lamellar structure is analogous to the nematic phase in liquid crystal. The type I shish transforms into type II shish (Figure 13C) by solidification of some parts of itself to form lamellar structure with no or undetectable periodicity. The type II shish further transforms into type III shish (Figure 13D) by the formation of more lamellar structure in itself. Well-defined periodicity appears with the increase of content of lamellar stacks. The barrier for the transformation from type I to type II shish or from type II to type III shish can be overcome by flow (strain) as evidenced by our results.

As aforementioned, several possibilities exist for the evolution of shish scattering intensity during isothermal process. Both dissolution of initial shish and generation of the shish may exist for all three types of shish. But in general, the isothermal process of type I shish mainly involves dissolution, which is consisted with the view of Hsiao et al.[42] and Balzano et al.[5] that the shish with defect or with size less than a critical value may dissolve back into melts due to the entropic recovery. On the contrary, the isothermal process of type III can be regarded as a generation process of new shish. The existence of shish precursor in deformed melts proposed by Kanaya et al.[31] and Ma et al.[28] seems in line with our

DOI: 10.1021/acs.macromol.5b00819
Macromolecules 2015, 48, 5276−5285

opinion. While the isothermal process of type II shish may be in between the cases of type I and type III shish.

CONCLUSION

In summary, we combine extension rheological and time-resolved SAXS measurements on PE blends with artfully designed thermal history to elucidate the formation process of shish nuclei. It is found that the critical strain for shish formation decreases with increasing UHMW component concentration, which agrees pretty well with the network model. Three types of shish appear sequentially with the increase of strain, exhibiting as the three stages in forming stabilized nuclei. The type I shish appears when stretch extent of UHMW component network reaching 0.46, which increases to 1 for the formation of type II shish. Our results clearly demonstrate the stretched network plays a major role in forming shish and support a kinetic process for shish formation from initial chain conformation to final stable nuclei. The segments couple with each other and pack into shish bundles when stretched to a critical value, then some parts of them solidify into sporadic lamellar structure with increasing the stretch extent. By further increasing the stretch extent and thus content of lamellar structure, the final stable shish form which contain lamellar stacks with well-defined periodicity. We believe that the realization of kinetic process for shish formation has profound implications for the tailoring of material properties from molecular principle and provides the underpinnings for theoretical models as well as enriches the study of FIC.

ASSOCIATED CONTENT

Supporting Information

These materials are available free of charge via the Internet at The Supporting Information is available free of charge on the ACS Publications website at DOI: 10.1021/acs.macromol.5b00819.

Additional results and analysis (PDF)

AUTHOR INFORMATION

Corresponding Authors

*(Z.W.) E-mail: zhangwh@ustc.edu.cn.

*(L.L.) E-mail: lbli@ustc.edu.cn.

Notes

The authors declare no competing financial interest.

ACKNOWLEDGMENTS

This work is supported by the National Natural Science Foundation of China (51325301, 51120135002 and 51227801), the Fundamental Research Funds for the Central Universities and the Project supported by NPL, CAEP (2013BB05). The experiment is partially carried out in National Synchrotron Radiation Lab (NSRL) and Shanghai Synchrotron Radiation Facility (SSRF).

REFERENCES

(1) Ward, I. M. *Makromol. Chem., Macromol. Symp.* **1988**, *22*, 59−82.

(2) Li, L. B.; de Jeu, W. H. *Interphases and Mesophases in Polymer Crystallization Ii* **2005**, *181*, 75−120.

(3) Somani, R. H.; Yang, L.; Zhu, L.; Hsiao, B. S. *Polymer* **2005**, *46* (20), 8587−8623.

(4) Kimata, S.; Sakurai, T.; Nozue, Y.; Kasahara, T.; Yamaguchi, N.; Karino, T.; Shibayama, M.; Kornfield, J. A. *Science* **2007**, *316* (5827), 1014−1017.

(5) Balzano, L.; Kukalyekar, N.; Rastogi, S.; Peters, G. W.; Chadwick, J. *Phys. Rev. Lett.* **2008**, *100* (4), 048302.

(6) Cui, K.; Meng, L.; Tian, N.; Zhou, W.; Liu, Y.; Wang, Z.; He, J.; Li, L. *Macromolecules* **2012**, *45* (13), 5477−5486.

(7) Phillips, A. W.; Bhatia, A.; Zhu, P. W.; Edward, G. *Macromolecules* **2011**, *44* (9), 3517−3528.

(8) Keller, A.; Kolnaar, J. W. H. *Prog. Colloid Polym. Sci.* **1993**, *92*, 81−102.

(9) Flory, P. J. *J. Chem. Phys.* **1947**, *15* (6), 397.

(10) Degennes, P. G. *J. Chem. Phys.* **1974**, *60* (12), 5030−5042.

(11) Mackley, M. R.; Keller, A. *Philos. Trans. R. Soc., A* **1975**, *278* (1276), 29−66.

(12) Mackley, M. R.; Keller, A. *Polymer* **1973**, *14* (1), 16−20.

(13) Okura, M.; Mykhaylyk, O. O.; Ryan, A. J. *Phys. Rev. Lett.* **2013**, *110* (8), 087801.

(14) Fernandez-Ballester, L.; Thurman, D. W.; Zhou, W.; Kornfield, J. A. *Macromolecules* **2012**, *45*, 6557.

(15) Balzano, L.; Rastogi, S.; Peters, G. *Macromolecules* **2011**, *44* (8), 2926−2933.

(16) Zuo, F.; Keum, J. K.; Yang, L.; Somani, R. H.; Hsiao, B. S. *Macromolecules* **2006**, *39* (6), 2209−2218.

(17) Ogino, Y.; Fukushima, H.; Matsuba, G.; Takahashi, N.; Nishida, K.; Kanaya, T. *Polymer* **2006**, *47* (15), 5669−5677.

(18) Heeley, E. L.; Fernyhough, C. M.; Graham, R. S.; Olmsted, P. D.; Inkson, N. J.; Embery, J.; Groves, D. J.; McLeish, T. C. B.; Morgovan, A. C.; Meneau, F.; Bras, W.; Ryan, A. J. *Macromolecules* **2006**, *39* (15), 5058−5071.

(19) Cui, K.; Meng, L.; Ji, Y.; Li, J.; Zhu, S.; Li, X.; Tian, N.; Liu, D.; Li, L. *Macromolecules* **2014**, *47* (2), 677−686.

(20) Matsuba, G.; Sakamoto, S.; Ogino, Y.; Nishida, K.; Kanaya, T. *Macromolecules* **2007**, *40* (20), 7270−7275.

(21) Zhao, B. J.; Li, X. Y.; Huang, Y. J.; Cong, Y. H.; Ma, Z.; Shao, C. G.; An, H. N.; Yan, T. Z.; Li, L. B. *Macromolecules* **2009**, *42* (5), 1428−1432.

(22) Seki, M.; Thurman, D. W.; Oberhauser, J. P.; Kornfield, J. A. *Macromolecules* **2002**, *35* (7), 2583−2594.

(23) Yan, T.; Zhao, B.; Cong, Y.; Fang, Y.; Cheng, S.; Li, L.; Pan, G.; Wang, Z.; Li, X.; Bian, F. *Macromolecules* **2010**, *43* (2), 602−605.

(24) Liu, D.; Tian, N.; Huang, N.; Cui, K.; Wang, Z.; Hu, T.; Yang, H.; Li, X.; Li, L. *Macromolecules* **2014**, *47* (19), 6813−6823.

(25) Zhang, C. G.; Hu, H. Q.; Wang, D. J.; Yan, S.; Han, C. C. *Polymer* **2005**, *46* (19), 8157−8161.

(26) Azzurri, F.; Alfonso, G. C. *Macromolecules* **2005**, *38* (5), 1723−1728.

(27) Azzurri, F.; Alfonso, G. C. *Macromolecules* **2008**, *41* (4), 1377−1383.

(28) Ma, Z.; Balzano, L.; Portale, G.; Peters, G. W. M. *Polymer* **2014**, *55* (23), 6140−6151.

(29) Cui, K.; Liu, D.; Ji, Y.; Huang, N.; Ma, Z.; Wang, Z.; Lv, F.; Yang, H.; Li, L. *Macromolecules* **2015**, *48* (3), 694−699.

(30) Zhao, Y.; Hayasaka, K.; Matsuba, G.; Ito, H. *Macromolecules* **2013**, *46* (1), 172−178.

(31) Deng, C.; Fujiwara, T.; Polec, I.; Matsuba, G.; Jin, L.; Inoue, R.; Nishida, K.; Kanaya, T. *Macromolecules* **2012**, *45* (11), 4630−4637.

(32) Liu, Y. P.; Zhou, W. Q.; Cui, K. P.; Tian, N.; Wang, X.; Liu, L. B.; Li, L. B.; Zhou, Y. G. *Rev. Sci. Instrum.* **2011**, *82* (4), 045104.

(33) Kisilak, M.; Anderson, H.; Babcock, N. S.; Stetzer, M. R.; Idziak, S. H. J.; Sirota, E. B. *Rev. Sci. Instrum.* **2001**, *72* (11), 4305−4307.

(34) Hammersley, A. P. *FIT2D V9.129 Reference manual v3.1, ESRF report 98HA01T*, 1998.

(35) Perret, R.; Ruland, W. *Acta Crystallogr., Part A* **1969**, *25*, S216.

(36) Nielsen, J. K.; Hassager, O.; Rasmussen, H. K.; McKinley, G. H. *J. Rheol.* **2009**, *53* (6), 1327.

(37) Coppola, S.; Grizzuti, N.; Maffettone, P. L. *Macromolecules* **2001**, *34* (14), 5030−5036.

(38) Wang, Y. Y.; Cheng, S. W.; Wang, S. Q. *J. Rheol.* **2011**, *55* (6), 1247−1270.

(39) Wagner, M. H.; Rolon-Garrido, V. H.; Nielsen, J. K.; Rasmussen, H. K.; Hassager, O. *J. Rheol.* **2008**, *52* (1), 67−86.

DOI: 10.1021/acs.macromol.5b00819
Macromolecules 2015, 48, 5276−5285

(40) Rubinstein, M.; Colby, R. H. *Polymer Physics*; Oxford University Press: New York, 2003.
(41) Mark, J. E. *Physical Properties of Polymers Handbook*; Springer Science+Business Media: New York, 2007.
(42) Keum, J. K.; Zuo, F.; Hsiao, B. S. *Macromolecules* **2008**, *41* (13), 4766−4776.
(43) Tian, N.; Zhou, W.; Cui, K.; Liu, Y.; Fang, Y.; Wang, X.; Liu, L.; Li, L. *Macromolecules* **2011**, *44* (19), 7704−7712.

DOI: 10.1021/acs.macromol.5b00819
Macromolecules 2015, 48, 5276−5285